

THE APPLICABILITY OF CFD TO SIMULATE AND STUDY THE MIXING PROCESS AND THE THERMO-HYDRAULIC CONSEQUENCES OF A MAIN STEAM LINE BREAK IN PWR MODEL

by

**Istvan FARKAS^a, Ezddin HUTLI^{b*}, Tatiana FARKAS^a,
Antal TAKACS^a, Ivan TOTH^a, and Attila GUBA^a**

^a Department of Thermo-hydraulics, Centre for Energy Research, Hungarian Academy of Sciences, Budapest, Hungary

^b Institute of Nuclear Techniques, Budapest University of Technology and Economics, Department of Thermohydraulics, Centre for Energy Research, Hungarian Academy of Sciences, Budapest, Hungary

Original scientific paper
<https://doi.org/10.2298/TSCI151126251F>

This paper focuses on the validation and applicability of CFD to simulate and analyze the thermo-hydraulic consequences of a main steam line break. Extensive validation data come from experiments performed using the Rossendorf coolant mixing model facility. For the calculation, the range of 9 to 12 million hexahedral cells was constructed to capture all details in the interrogation domain in the system. The analysis was performed by running a time-dependent calculation. Detailed analyses were made at different cross-sections in the system to evaluate not only the value of the maximum and minimum temperature, but also the location and the time at which it occurs during the transient which is considered to be indicator for the quality of mixing in the system. CFD and experimental results were qualitatively compared; mixing in the cold legs with emergency core cooling systems was overestimated. This could be explained by the sensitivity to the boundary conditions. In the downcomer, the experiments displayed higher mixing: by our assumption this related to the dense measurement grid (they were not modelled). The temperature distribution in the core inlet plane agreed with the measurement results. Minor deviations were seen in the quantitative comparisons: the maximum temperature difference was 2°C.

Key words: *mixing, coolant, main steam line break, cold-leg, temperature, loss-of-coolant accident, pressurized water reactor, density, emergency core cooling, reactor pressure vessel*

Introduction

In the case of a loss-of-coolant accident (LOCA) of pressurized water reactor (PWR), the emergency cooling water system is used to feed the primary loops (cold legs) with additional water (coolant) in order to secure core cooling. Injected water mixes with hot primary coolant and flows into the pressure vessel. After reactor shut-down the temperature of coolant in reactor pressure vessel (RPV) and in the connecting pipes could be above 200 °C while the emergency core cooling systems (ECCS) water may be around 50 °C. In order to reduce the LOCA side effects, the question of how well cold and hot liquids mix in the primary coolant

*corresponding author; e-mail: ezddinhutli@yahoo.com

loops must be answered. Due to the large temperature difference between cold leg and ECCS injection, the fluid densities differed by about 20%. In such a case the resulting flow pattern is governed primarily by buoyancy forces, *i. e.* thermal stratification and mixing of the cold and hot water play a dominant role [1-3]. As a result of insufficient mixing process between the ECC water and that in the cold leg, some of injected water flows at the bottom of the cold leg. The cold layer is formed and thermal stratification is a result. When the stratification phenomenon forms in the cold leg, steam condensation on injected water occurs, and local pressure variations cause unstable flow oscillations, which promotes coolant mixing. The main three consequence safety problems related to poor mixing process in the cold leg and RPV are boron dilution, pressurized thermal shock (PTS), and thermal fatigue (TF). The first consequence is the boron dilution transients in the reactor core leading to reactivity insertions, which possibly leads to a power increase [4, 5]. The second consequence is the PTS scenario which is limiting the RPV lifetime. PTS denotes the occurrence of thermal loads on the RPV under pressurized conditions. These thermal loads may lead to very large stresses and to the instability of latent damage present inside the vessel wall. Therefore, assessment of PTS is important for long term operation, since the integrity of the RPV has to be assured throughout the lifetime of the reactor [6, 7]. Third consequence is the TF phenomenon. It is a degradation mechanism induced on the primary system of a nuclear power plant. Consequences of thermal fatigue are often very critical, ranging from structural damage to a complete shut-down as happened with the French Civaux reactor in 1998. The temperature fluctuations that arise from irregular turbulent mixing of hot and cold flows cause stress fluctuations in the solid structures, which lead to fatigue damage. Due to the high frequencies involved, these three phenomena are difficult to detect by common plant instrumentation, numerical simulations are therefore needed, associated if possible with non-intrusive measurement techniques such as particle image velocimetry (PIV) and laser induced fluorescence (LIF) [8, 9]. At the Centre for Energy Research (EK) in Budapest a work using both numerical and measurement techniques to investigate the flow dynamic and temperature distribution field for the safety assessment has been published [3, 10, 11]. More detailed analysis of the cold leg/upper downcomer region has been performed based on experimental and calculation results, comparing different numerical methods. Numerical and experimental studies have been performed in the past to assess flow mixing behavior in normal and transient situation. Many researchers have been investigating this area, among them Pochet *et al.* [12] showed that the main mixing phenomena are qualitatively in good agreement with experimental results, but quantitatively the deviations are exist. In the work of Yamaji and Aszodi [13] 3-D CFD calculations, the results of the calculations reproduced qualitatively well the measured data, while quantitatively a significant difference was observed. They assumed that the investigation of such mixing processes can be sensitive to the level of discretization. Hohne and Soren [14] investigated the phenomenon experimentally and numerically. They concluded that when the stratified flow is developing during the injection in the cold leg and in the downcomer, first the momentum driven flow field, then the density has the big effects. Vaibar and Hohne [15] combined numerical and experimental study of buoyant mixing processes. The obtained results showed that, the main influence on the accuracy of the result is the simplification of the flow domain. The proper flow domain leads to a better agreement between the numerical and experimental results. Many of published works investigate the applicability of Unsteady Reynolds-Averaged Navier–Stokes (URANS) equations simulation to predict the mixing phenomena and their side effects. As an example, Gango [16] studied the boron mixing process in the downcomer using a CFD code Phoenix. Hohne *et al.* [17] studied the influence of density differences on the mixing of the primary loop and the ECCS in the Rossendorf coolant mixing model (ROCOM)

facility using a Reynolds stress model (RSM) in the CFX-5 code. Rohde *et al.* [1] performed detailed CFD code validations for fluid mixing in a primary circuit of a PWR. Dury *et al.* [18] studied a boron dilution event using different simulation techniques in the CFX-5. The results were compared with these obtained using a 1/5th-scale, 3-loop PWR facility. Other published, related work has been done using large eddy simulation (LES) which represents a more advanced turbulent model. Among them, Hohne *et al.* [19] demonstrated the applicability of LES to predict the low patterns and mixing phenomena, Loginov *et al.* [20, 21] studied the grid and accuracy requirements for applied LES, Ducros *et al.* [22] presented that, the LES could be used as a tool for the analysis of boron dilution transients under weak mixing process condition, and Jayaraju *et al.* [23] investigated the validation and applicability of large eddy simulation (LES) to analyze the transport and mixing in the RPV. The qualitative comparisons to the ROCOM experimental data showed good predictions by the LES model while small deviations appear in the quantitative comparisons. In addition, they presented a brief review of the related publications which gave a valuable help to us in the writing the introduction of this paper Hutli *et al.* [24] investigated the mixing process in a model of reactor vessel down-comer and in cold leg inlets using PIV, LIF, and CFD techniques. The obtained results show that, the influence of mixing process on the outlet temperature profile, and the CFD results shows acceptable agreement with measurement results.

In this paper the URANS computation models is used to predict the mixing phenomena in different cross-sections in the primary loop. It Also presented the simulated ROCOM experiments 1.2 which include the CFD model, mesh generation methodology and the sensitivity of the obtained results to these parameters. The comparison of calculations with the experimental data is also presented, and the main conclusions and future perspectives of the study are in the end of the paper.

Description of calculation model

In order to simulate the experiments in FLUENT, the already existing ROCOM model had to be completed by the ECCS and by longer cold legs. The analysis was performed by running a time-dependent calculation. Due to the complexity and the extent of the geometry of ROCOM facility, the meshing was a key task during the model design and its development. The calculation model of ROCOM experiments 1.2 was applied using the numerical mesh of the previous work [1]. The numerical mesh was built up gradually performing test calculations in order to obtain a good result associated with correctness of the process during the calculation steps. The generated mesh consisted the range of 9 to 12 millions of hexahedral cells. The cold leg 3 and 4 of the model were extended and supplemented by the pipe of the safety injection system. The numerical mesh consisted of hexahedral cells exclusively and its quality corresponded to recommendations of BPG [6]. Figure 1 shows the numerical mesh of the cold leg and the nozzle of safety injection system. Reasonable attention was given to components which significantly influence the velocity field, *i. e.* the mixing process, such as the core barrel with the lower core support plate and core simulator, perforated drum in the lower plenum, and inlet and outlet nozzles. In the first step the calculation domain and modelling were done for the downcomer

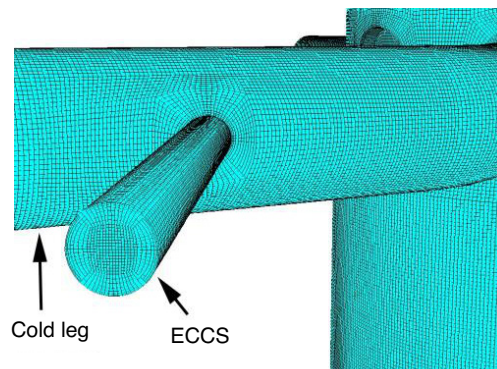


Figure 1. Details of the numerical mesh

and the connecting cold leg nozzles as shown in fig. 2(a)-(c). In the course of problem solving three geometrical versions of calculation model were used, differing in the length of cold legs. Steady-state calculation (initialization of transient calculation) was done on the largest scale model, fig. 2(a), to get initial state for the further transient calculation. The generated mesh consisted of around 12 million hexahedral cells. For the steady-state calculation the boundary conditions used were the coolant temperature at the four cold legs are equal ($T_{1,2,3,4} = 227.60$ °C), and velocity at cold legs 1, 2, and 4 are equal ($V_{1,2,4} = 0.0662$ m/s), while the velocity at cold leg 3 is different ($V_3 = 0.1765$ m/s), the injection velocity at ECC is assumed to be zero ($V_{inj} = 0$ m/s).

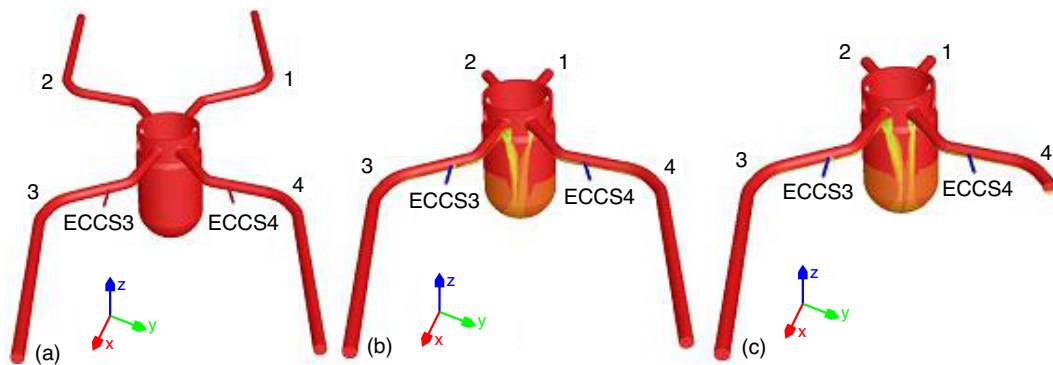


Figure 2. Calculation models of the experiments facility for; (a) initial state: vessel, cold legs, and safety injection nozzles, (b) model used for the first 50 second of transient calculation, (c) model used after the first 50 second of transient calculation (for color image see journal web site)

Average velocity of coolant was defined at the boundaries since no measurement was performed for velocity distribution. To compensate this simplification, the legs were modelled with such lengths which form fully developed velocity profiles in the coolant even before the bends in legs. Length of cold leg was decreased, fig. 2(b), in loops 1 and 2. In transient simulation there was no safety injection and then velocity and turbulence profiles were set as initial conditions from steady-state (by this way we reduced the time of calculation). This procedure could not be followed in loops 3 and 4 because in them the greater density water of safety injection (ECC) spreads on the bottom of the leg and only a part of it flows toward the vessel. The another part of it causes backflow which has an extent (no available data). So the length of these legs was not changed. For the transient case, calculation of the mesh used here contains 8.896536 million cells under the boundary conditions; as follows: $V_{1,2}$: velocity profiles from preliminary simulation, $T_{1,2,3,4} = 227.60$ °C, the injection velocity at ECC is increased for both cold legs (3 and 4) $V_{inj} = 0.4138$ m/s, $V_3 = 0.1765$ m/s, $V_4 = 0.0662$ m/s. A third version of the numerical model was developed, fig. 2(c), because in loop 4 with the lowest flow rate, the part of injected ECCS cold water reaches the location where boundary condition of not shortened leg 4 was given. According to the simulation, this phenomenon happens after 50 seconds affecting instability in the calculation. As prolongation of this leg should solve the problem only temporarily we decided to eliminate it by shortening. For this purpose was selected a section between ECCS connection and the inlet where the flow conditions were supposed to be constant for the remaining part of simulation. Profiles of velocity, turbulence and temperature developed in this section were used for new inlet boundary conditions of the shortened cold leg 4. The other boundary conditions were kept identically, the used mesh contained 8.128416 million cells. The overestimated back flow phenomenon did not exist in cold leg 3 because of higher flow rate in this leg. This result shows the influence of injection flow rate in the mean pipe [10].

Test calculations procedures, results, and comparison with measurements

Calculation consisted of three parts like ROCOM experiment itself with arrangements as described earlier. In the first part of calculation, the steady state of the test was reproduced by steady-state calculation where coolant circulated in the loops with specified flow rates. In the beginning, $k-\varepsilon$ turbulence model was applied and the porosity was neglected at the perforated barrel (drum). As soon as this simplified calculation had converged, we changed to the more developed and more generally applicable RSM turbulence model and then we switched on porosity in the region belonging to the perforated barrel. In this phase of the experiment there was still no ECCS injection so the density (salt content) was homogeneous and sensors could not be used. Calculation results have been considered suitable based on decrease and stability of residual values. ECCS injection and measurement started after stabilization of flow profile in the legs. This part of the test lasted till the flow profile and temperature (concentration) nearly stabilized again in accordance with the new conditions. In experiments time this process took 60 seconds. The simulation was performed as a transient calculation using the steady state results of the first part. The good parameter that could be used to describe and control the system is the coolant flow rate averaged temperature at the outlet boundary condition because its stabilized value can be obtained from the heat balance (energy balance). The outlet average temperature in fig. 3 shows a convergence toward the stabilized value but does not reach it even by the end of the test. Because of technical reasons, the stabilization of the system could not be reached in the experiment, so the third part of the test can be regarded as quasi-steady. The calculation had to be continued as a transient. Temporary fluctuations of parameters were filtered by time between 60 and 70 seconds. These average values were compared at experiments sensors position (experimental results at that positions), their positions are denoted by coloured surfaces in fig. 4. at core inlet, in the downcomer and in legs 3 and 4 in three-three cross-sections.

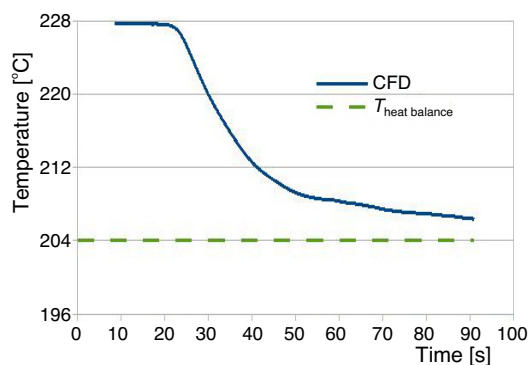


Figure 3. The evolution of outlet average temperature vs. time

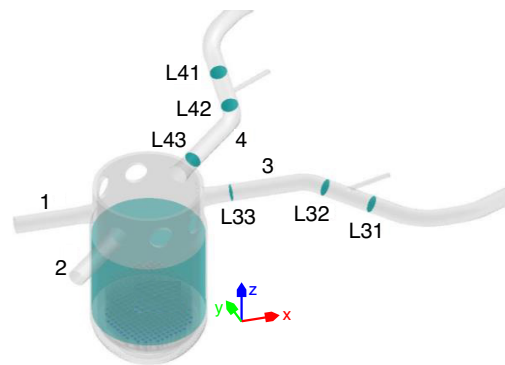


Figure 4. Positions of the sensors at core inlet, in downcomer and in legs 3 and 4 in experiments (for color image see journal web site)

Temperature profiles (distribution) in measured legs can be seen in figs. 5 and 6. Upper group (first row) displays calculation results and lower group (second row) shows experiment results. The dimensionless temperature profile cross-sections were identified by the name of the sensors as presented in fig. 4. From figure top downwards cross-sections (L31-L32-L33) approach the vessel. No measurement data were given in the cross-section of leg 3 furthest from the vessel because the cold water from ECCS did not reach this cross-section in the experiments

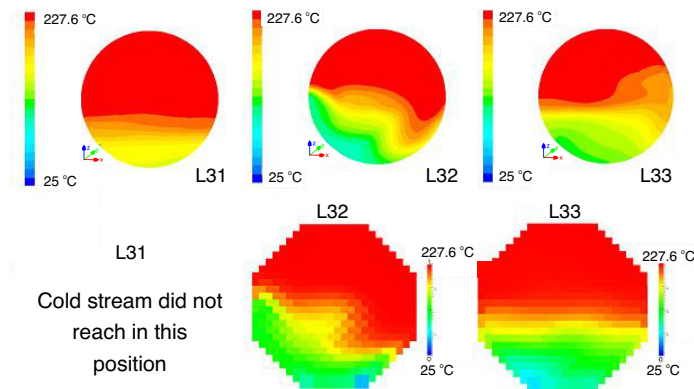


Figure 5. Dimensionless temperature profiles in cold leg 3 at cross-sections (L31-L32-L33) approach the vessel; first row – calculation results, second row – measurements results
(for color image see journal web site)

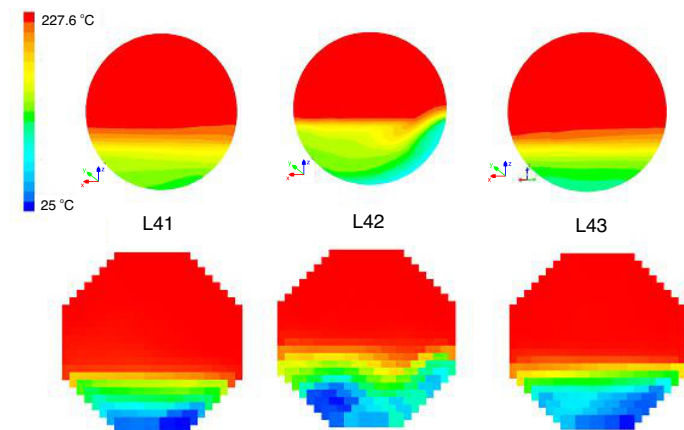


Figure 6. Dimensionless temperature profiles in cold leg 4 at cross-sections (L41-L42-L43) approach the vessel; first row – calculation results, second row – measurement results
(for color image see journal web site)

0.18. This value belonged to just one measurement point around which higher temperature values could be observed (0.4). The relative temperature is defined as $T_{rel} = (T - T_{min}) / (T_{max} - T_{min})$ (where T_{rel} is a relative temperature, T – the calculated or measured temperature at any point, $T_{min} = 25^\circ\text{C}$ and $T_{max} = 227.65^\circ\text{C}$). Deviations may be caused also by a partial backflow of cold water in the calculation. In fig. 6 experiments and calculated temperature profiles of lower flow rate in leg 4 are shown. In section L41 furthest from reactor vessel one can see that the backflow is more significant than in leg 3. Isotherm layers were close to horizontal here as well. The location of the lowest temperature agreed in the experiments and the calculation. At the same time its value was much lower in the experiments. This fact refers to an overprediction of mixing by the calculation. In section L42 temperature stratification slightly differs in experiment and calculation. In the experiments the injected water forms greater waves in the temperature field. The coldest layer runs up to the right side of the leg both in the experiments and calculation, while in the experiments this layer is more extended on the left side as well, moreover, its coldest part is colder than in the cal-

(L31). However, even in this leg with higher flow rate the injected water of higher density caused such a strong backflow in the bottom of the cold leg that it reached section L31 in the calculation.

The backflow water significantly heats up till reaching L31 but its momentum was only sufficient to get to the bend above the studied section. From here it turned back due to the flow toward the vessel (fig. 7). Experiments and calculation temperature profiles are in good agreement in section L32 below ECCS connection in the main direction of the flow. Both experiments and calculation data show a leaning, almost 45° , isotherm layers are formed as the cold water injected from aside swings over the left side of the leg. Middle density water emerges from among layers in the internal of the section and flows toward the bottom of the leg wavelike. The calculated minimum of the relative temperature field was 0.37 while the minimum in experiments was

culatation flows. In the cross-section closest to the vessel (L43) the calculation predicts correctly the temperature layers are leaning slightly to the left which is also observable in the experiments. The minimum of the temperature in the experiments is also lower just as in other leg sections, the calculation overpredicted the mixing. A possible reason of the overprediction may be related to the uncertainty in the injection boundary conditions or numerical diffusion generated by application of first order discretization scheme [13]. Despite quantitative discrepancies, the simulation reflected the temperature distribution of legs qualitatively well.

Figure 8 presents the experiment and calculation temperature fields in the downcomer and on internal/external measurement surfaces. Simulation reflects the lowest temperature location qualitatively and quantitatively well at the top external measurement surface below loop 4. The major part of cold water from ECCS injection differently from RO-COM experiments 1.1 with higher flow rate in our earlier study [1] remains in the external part of the downcomer, fig. 9, and reaches the core barrel (support basket) just to a smaller extent. There is a weaker mixing in loop 4 with lower flow rate so the injected water warms up but less than that in leg 3. In turn the colder plume heads for the bottom of the vessel with a greater acceleration when entering than the cold plume of lower density from leg 3. The pressure decreases around the colder plume with greater acceleration so it affects the other plume as drives the other plume toward itself. In the experiments these plumes met by the bottom of the vessel. Numerical comparison of temperature data are shown in figs. 10 and 11. Azimuthal reference lines on applied external measurement surface are displayed by black line in figs. 8 and 9. On the upper line the calculation reflects well

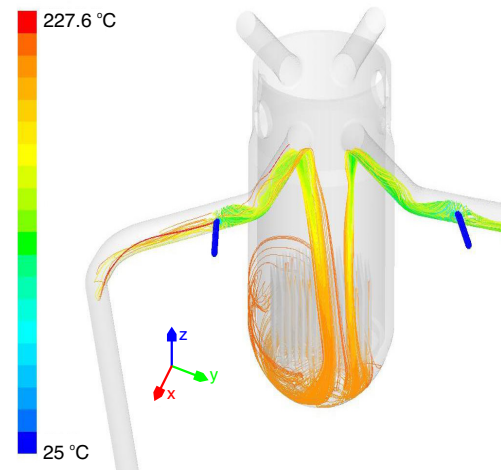


Figure 7. Streamlines of the total flow are coming from cold legs 3 and 4 and others streamlines are coming from ECCS lines. Part of injected ECCS of leg 3 is turned back, the lines are coloured according to thier temperature (for color image see journal web site)

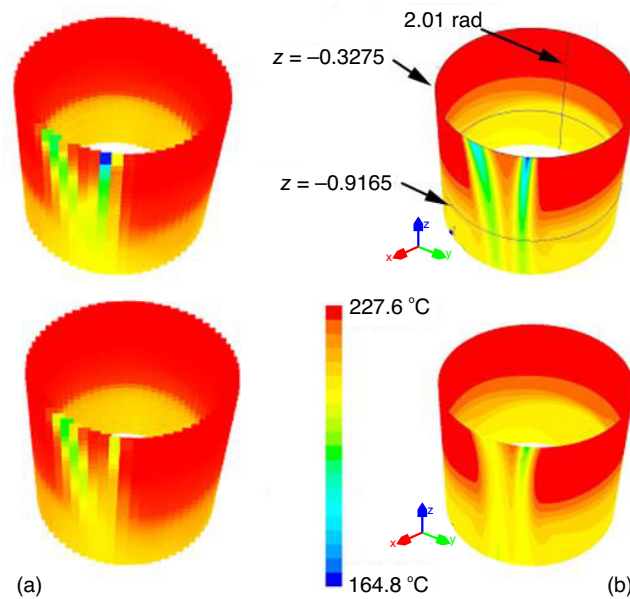


Figure 8. Temperature distribution in the downcomer, at external (top at $z = -0.3275$ m) and internal (bottom at $z = -0.9165$ m) sensor position; (a) measurement, (b) calculation (z in m) (for color image see journal web site)

Figure 8 presents the experiment and calculation temperature fields in the downcomer and on internal/external measurement surfaces. Simulation reflects the lowest temperature location qualitatively and quantitatively well at the top external measurement surface below loop 4. The major part of cold water from ECCS injection differently from RO-COM experiments 1.1 with higher flow rate in our earlier study [1] remains in the external part of the downcomer, fig. 9, and reaches the core barrel (support basket) just to a smaller extent. There is a weaker mixing in loop 4 with lower flow rate so the injected water warms up but less than that in leg 3. In turn the colder plume heads for the bottom of the vessel with a greater acceleration when entering than the cold plume of lower density from leg 3. The pressure decreases around the colder plume with greater acceleration so it affects the other plume as drives the other plume toward itself. In the experiments these plumes met by the bottom of the vessel. Numerical comparison of temperature data are shown in figs. 10 and 11. Azimuthal reference lines on applied external measurement surface are displayed by black line in figs. 8 and 9. On the upper line the calculation reflects well

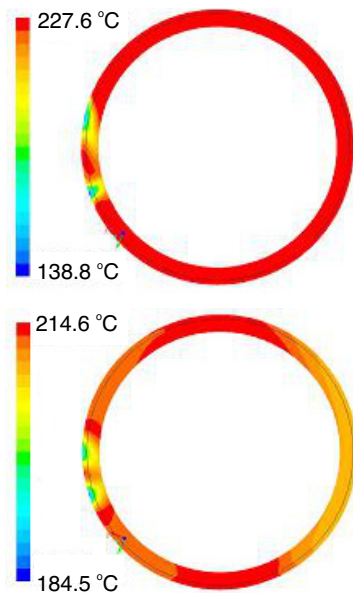


Figure 9. Simulated temperature field emerging in the downcomer at $z = -0.3275$ m (upper one) and $z = -0.9165$ m (lower one) (for color image see journal web site)

the results of the experiment a bit surprisingly if we consider differences among legs. Simulation overpredicted mixing in the legs but this discrepancy disappeared when cold water reached the downcomer. This is only possible if somehow the mixing was increased in the experiment. We assume that this effect was induced by the applied measurement grids. This assumption is confirmed by the fact that numerical comparison in the bottom of the downcomer, fig. 11, shows some deviation. The coolant crosses the measurement grid in the downcomer, the mixing process is enhanced in the experiments at this part (bottom of the downcomer) the result is this kind of deviation, fig. 11. At this level the plumes met and the temperature profile smoothed. Hot water layer in the top part of the reactor vessel is fed by legs 1 and 2. The width of this layer is greater than that in the simulation just like in ROCOM experiments 1.1. This difference is not so great as we had experienced before for greater flow rate [1] according to numerical comparison made along the vertical reference line, fig. 12. The fact that this effect decreased with the velocity of the flow just like the supposed hydraulic resistance, also refers to the disturbing phenomenon of the measurement grid.

Temperature vs. time in 4 time points is displayed in figs. 13 and 14 along the vertical reference line chosen between cold legs 1 and 2, fig. 8. Experiments results can be considered regular which refers to a stronger instantaneous stability in experiment than in simulated values. The shape of temperature profiles were similar and did not cross each other. On the contrary, temperature profiles of the calculation have different shapes occasionally crossing each other (fig. 13) which implies an instability in the flow. Having a closer look at streamlines in fig. 7, we can see that, similarly to the earlier ROCOM experiments [1] the coolant flow downwards also forms 1-1 circulations on the sides of the flow compensator barrel. The two circulation zones meet on the opposite side of the barrel between loops 1 and 2 (at the chosen reference line) to make the developed flow slightly unstable. This profile is verified by the temperature evolution in time belonging to the crossing of reference lines, fig. 15, where greater fluctuations occurred in the calculation. However, the assumed hydraulic resistance in the experiments could mitigate this instability.

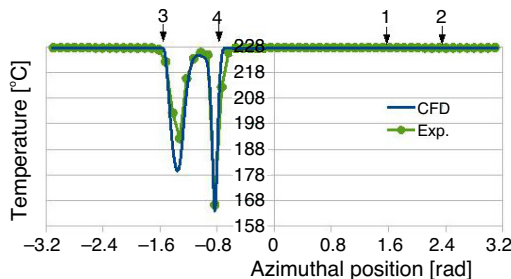


Figure 10. Temperature distribution along the perimeter of the downcomer, 0.3275 m away from the centerline of cold nozzles ($z = -0.3275$ m)

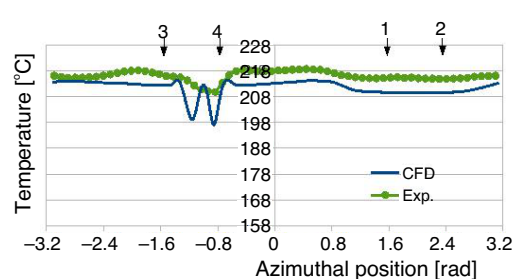


Figure 11. Temperature distribution along the perimeter of the downcomer, 0.9165 m away from the centerline of cold nozzles ($z = -0.9165$ m)

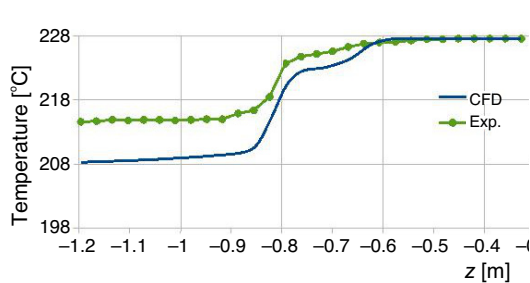


Figure 12. Calculated and measured temperature distribution along vertical “2.01rad” line in the downcomer temperature distributions were compared as time averaged values between 60 and 70

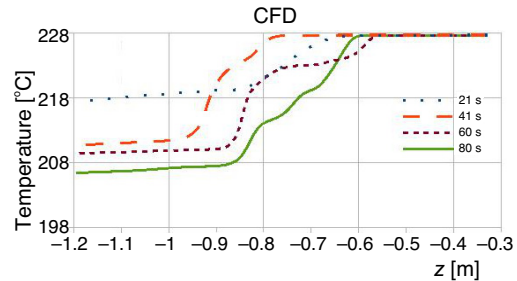


Figure 13. Calculated temperature distribution along vertical “2.01rad” line chosen between cold legs 1 and 2 in the downcomer at four time points

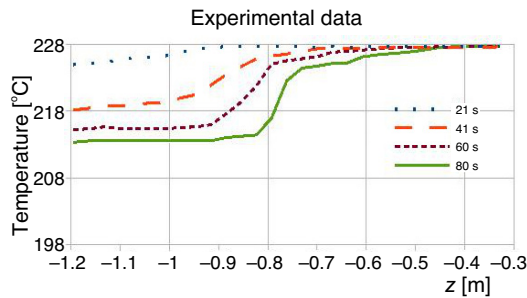


Figure 14. Measured temperature distribution along vertical “2.01rad” line in the downcomer cold legs 1 and 2 in the downcomer at four time points

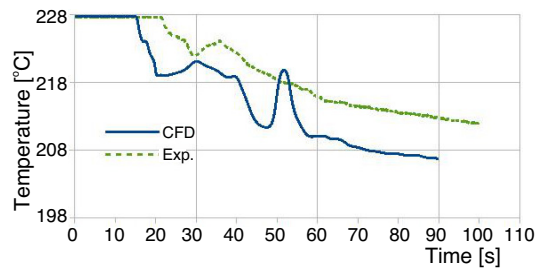


Figure 15. Temperature evolution at the cross point of the two references lines (“2.01rad” and $z = 0.9165$ m) in the downcomer

The measured and calculated temperature distribution at core inlet is almost homogeneous, showing around 2 °C difference between minimum and maximum values in both cases, fig. 16, except for the experiments temperature scale shifted up with around 7 °C. This discrepancy could also be observed in the downcomer. In the experiments the coldest point occurred close to loop 4 while at loop 3 for the calculation. This can be explained with temporary azimuthal temperature profiles of the downcomer shown in figs.17-19. According to this, the coldest point slowly shifts from cold legs 3 and 4. But this process is slower in the calculation and develops only in 80 s after the averaged time interval. The hot measured point in the experiments can be found at core inlet boundary between loops 3 and 2 while below loop 1 in the calculation. Despite differences experienced at core inlet one can notice that local extrema of the temperature field approach each other. Temperature evolution at core inlet center was also examined (fig. 17). The temperature starts to decrease earlier in the calculation, the measured value follows this trend with some seconds delay. The trend of results shows some divergence as experiments and calculation results tend to different values. In figs. 11, 12, 15 and 18, one can notice that measured temperature values exceed calculated ones with 0.2-0.4 on the average. In our understanding this inaccuracy is supposed to come from applying water density vs temperature exactly in the calculation while in the experiments this material law might be linear since temperature was experimentally modelled by density/concentration of salt solution. This supposition remained unproved because exact correlation was not given in the specification of the experiments but according to our estimation based on heat and concentration balance, the discrepancy might have developed in the examined temperature interval.

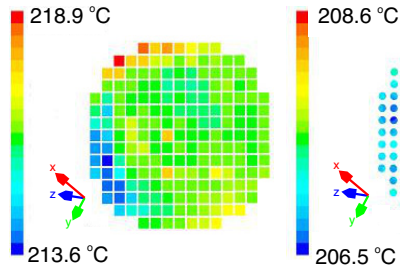


Figure 16. Temperature distribution at core inlet (left – experiments, right – calculation) (for color image see journal web site)

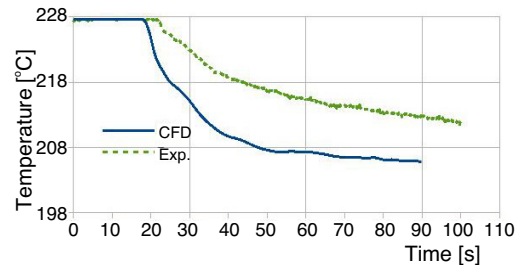


Figure 17. Temperature evolution in time at center of the core inlet

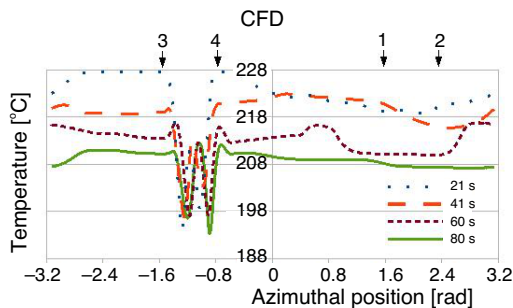


Figure 18. Calculated temperature distribution along azimuthal line at $z = -0.9165$

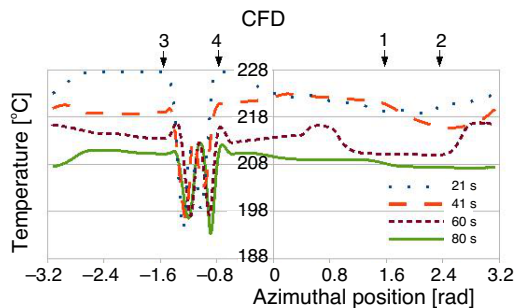


Figure 19. Experiments temperature distribution at azimuthal line at $z = -0.9165$

Conclusions

The CFD model of the ROCOM facility was expanded and transformed to facilitate the calculation of ROCOM experiments 1.2. Preliminary calculations have been performed with this new model to determine inlet velocity and turbulence profiles in cold legs. Since the steady-state could not be achieved in the measurements due to technological reasons, the simulation of the experiments was done with transient solver. The time averaged results and their time evolutions were compared. The fact that calculated temperature fields showed good qualitative agreement with the measurements shows that our CFD simulation reflected appropriately this case with low flow rate. The quantitative differences might come from insufficient specification of boundary conditions like ECCS entrance or hydraulic resistance of measurement grids or that the density change of the coolant due to temperature change was experimentally modelled with salt concentration. Experimental data were distributed in the form of the temperature data. The calculation was performed with real non-linear material laws of water vs temperature and the solution of energy equation. This difference can be neglected in narrow temperature intervals as it did not count too much in ROCOM experiments 1.1 but here the greater temperature differences can affect calculation results. The calculation performed over-predicted ECCS mixing in the legs. However, experiments evidenced a more intensive mixing in the downcomer. The difference between calculated minimum and maximum temperatures was around 2 °C which agreed exactly with measurement results. Results at core inlet are satisfactory from the point of view of nuclear safety because they reflected well the homogeneous distribution of the coolant. Since the future goal of the task is to decrease conservatism applied in reactor vessel, pressurized thermal shock (PTS) studies, it would be worth while to continue

studies based on experimental data base available to us. In these studies detailed calculations should be performed separately for the downcomer and for the upper part of the downcomer too, comparing the results of different numerical modelling methods. Such kind of possibility is e. g. the replacement of the URANS approach applied here by LES. This step requires a considerable increase of numerical mesh resolution which also increases necessary calculation capacity and so may reduce studies to smaller chosen parts of the model.

Acknowledgment

The authors gratefully acknowledge the support of all national and international organizations participated in the PKL project mainly who worked on ROCOM facility. Their valuable feedback on the test result was helpfully supported in the interpretation and final evaluation of the calculation. The author also grateful for the support of the Hungarian Atomic Energy Authority (OAH).

References

- [1] Rohde, U., et al., Fluid Mixing and Flow Distribution in a Primary Circuit of a Nuclear Pressurized Water Reactor Validation of CFD Codes, *Nuclear Engineering and Design*, 237 (2007), 15-17, pp. 1639-1655
- [2] ***, Helmholtz-Zentrum Dresden-Rossendorf, Experimental Studies of the Fluid Dynamics during a Pressurized Thermal Shock (PTS), <https://www.hzdr.de/db/Cms?pOid=25292&pNid=3016>
- [3] Farkas, T., Toth I., Fluent Analysis of a ROSA Cold Leg Stratification Test, *Nuclear Engineering and Design*, 240 (2010), 9, pp. 2169-2175
- [4] Kiger, K. T., Gavelli, F., Boron Mixing in Complex Geometries: Flow Structure Details, *Nuclear Engineering and Design*, 208 (2001), 1, pp. 67-85
- [5] Rohde, U., et al., Fluid Mixing and Flow Distribution in the Reactor Circuit, Measurement Data Base, *Nuclear Engineering and Design*, 235 (2005), 2-4, pp. 421-443
- [6] ***, IAEA-TECDOC-1627, Pressurized Thermal Shock in Nuclear Power Plants: Good Practices for Assessment, Deterministic Evaluation for the Integrity of Reactor Pressure Vessel. International Atomic Energy Agency Vienna, 2010, http://www-pub.iaea.org/MTCD/publications/PDF/te_1627_web.pdf
- [7] Jiejun, C., Tadashi, W., Numerical Simulation of Thermal Stratification in Cold Legs by Using Open-FOAM, *Progress in Nuclear Science and Technology*, 2 (2011), Oct., pp. 107-113
- [8] Nobuchika, K., et al., Spectra Thermal Fatigue Tests under Frequency Controlled Fluid Temperature Variation: Transient Temperature Measurement Tests, *Proceedings*, ASME Pressure Vessels and Piping/ICPVT-11 Conference, 2006, Vancouver, Canada, pp. 857-864
- [9] Courtin, S., High Cycle Thermal Fatigue Damage Prediction in Mixing Zones of Nuclear Power Plants: Engineering Issues Illustrated on the FATHER Case, 5th Fatigue Design Conference, Fatigue Design, *Procedia Engineering*, 66 (2013), Feb., pp. 240-249
- [10] Gottlasz, V., et al., Measuring of Velocity and Temperature Field in a Model of Reactor Vessel Downcomer and Cold-Legs Inlets, *Proceedings*, 10th International Symposium on Particle Image Velocimetry – Delft, The Netherlands, 2013
- [11] Hutli, E., et al., 2013. Investigation of Mixing Flow Process Using PIV and PLIF Techniques, *Advanced Materials Research*, 816-817 (2013), Sept., pp. 1054-1058
- [12] Pochet, G., et al., CFD Simulations of Buoyancy Driven Flow Mixing Experiments Performed at the Rocom Facility, *Proceedings*, 14th International Topical Meeting on Nuclear Reactor Thermal Hydraulics (NURETH-14), 2011, Toronto, Canada, pp. 1-12
- [13] Yamaji, B., Aszodi, A., CFD Analysis of Coolant Mixing in VVER-1000 Pressure Vessel, *Proceedings*, 16th Symposium of AER on VVER Reactor Physics and Reactor Safety, Bratislava, Slovakia, 2006, pp. 483-491
- [14] Hohne, T., Soren, K., Modeling of a Buoyancy-Driven Flow Experiment in Pressurized Water Reactors Using CFD Methods, *Nuclear Engineering and Technology*, 39 (2007), 4, pp. 327-336
- [15] Vaibar, R., Hohne, T., Buoyancy Driven Flow in Reactor Safety, *Applied and Computational Mechanics*, 3 (2009), pp. 22-232
- [16] Gango, P., Numerical Boron Mixing Studies for Loviisa Nuclear Power Plant, *Nuclear Engineering Design*, 177 (1997), 1-3, pp. 239-254

- [17] Hohne, T., *et al.*, Boron Dilution Transients During Natural Circulation Flow in PWR Experiments and CFD Simulations, *Nuclear Engineering Design*, 238 (2008), 8, pp. 1987-1995
- [18] Dury, T. V., *et al.*, CFD Simulation of the Vattenfall 1/5th-Scalepwr Model for Boron Dilution, *Nuclear Engineering Design*, 238 (2008), 3, pp. 577-589
- [19] Hohne, T., *et al.*, Modeling of a Buoyancy-Driven Flow Experimental the ROCOM Test Facility Using the CFD Codes CFX-5 and Trio-U, *Nuclear Engineering Design*, 236 (2006), 12, pp. 1309-1325
- [20] Loginov, M., *et al.*, Application of Large-Eddy Simulation to Pressurized Thermal Shock, a Grid Resolution Study, *Nuclear Engineering Design*, 240 (2010), 8, pp. 2034-2045
- [21] Loginov, M., *et al.*, Application of Large-Eddy Simulation to Pressurized Thermal Shock: Assessment of the Accuracy, *Nuclear Engineering Design*, 241 (2011), 8, pp. 3097-3110
- [22] Ducros, F., *et al.*, Verification and Validation Considerations Regarding the Qualification of Numerical Schemes for LES for Dilution Problems, *Nuclear Engineering Design*, 240 (2010), 9, pp. 2123-2130
- [23] Jayaraju, S. T., *et al.*, Large Eddy Simulation for an Inherent Boron Dilution Transient, *Nuclear Engineering and Design*, 262 (2013), Sept., pp. 484-498
- [24] Hutli, E., *et al.*, Experimental and Numerical Investigation of Coolant Mixing in a Model of Reactor Pressure Vessel Down-Corner and in Cold Leg Inlets, *Thermal Science*, 21 (2017), 3, pp. 1491-1502